GaN-HEMT on Si as a Robust Visible-blind UV detector with High Responsivity

Arathy Varghese, Abdalla Eblabla, Zehao Wu, Seyed Urman Ghozati, and Khaled Elgaid

Abstract—**This work presents performance evaluation of GaN High Electron Mobility Transistor (HEMT) based ultraviolet (UV) detector on Si substrate. In addition to the fabrication and characterization, a systematic study is presented here using simulations extensively to investigate the UV detection mechanism. Output current has been chosen as the sensing metric, the fabricated device exhibits a high UV responsivity of 1.62×10^7 A/W at 2.5×10^{-10} W, V_{GS}=0.5 V. Simulations have been done using optical modules available in Silvaco ATLAS TCAD to analyze the energy band bending, Two-Dimensional Electron Gas (2DEG), channel potentials and electric fields in the device. This model can aid in systematic study of HEMT based detectors in terms of dimensional and epi layer design optimizations for sensitivity enhancements. The UV response of the device is found to decrease as the wavelength approaches the visible light wavelength. This makes the photodetectors blind to visible light ensuring selective detection of UV wavelengths. It has been observed that as the area for UV absorption is increased by increasing the W/L ratio, the increases. For a W/L ratio of 100, the detector exhibits a responsivity of 1.86×10^7 A/W.**
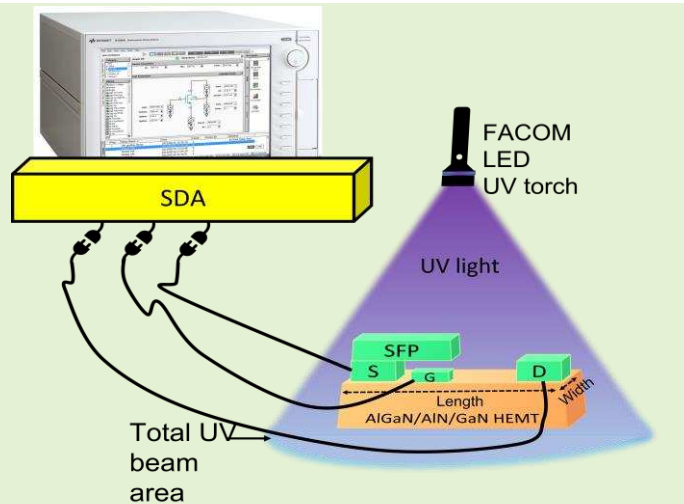
Index Terms— **AlGaN/GaN HEMT; sensor; sensitivity; UV detection; photodetector.**

I. INTRODUCTION

GALLIUM nitride electronics has gained huge attention in recent years due to its inherent advantages of the wide band gap material and Two-Dimensional Electron Gas (2DEG) formation when an AlGaN/GaN heterojunction is grown [1, 2]. High frequency power electronics, optical and sensing technology are the three main application domains of GaN based devices [3-6]. Recent years have seen an increased interest in development of UV detectors due to their increased demands in military, civil and space applications [7, 8]. Amongst these, in this era of human beings moving towards becoming an interplanetary species, space ozone monitoring is of great importance and Si based detectors fail at these high temperatures. The solution lies in wide band gap devices that exhibits ruggedness and higher resilience to radiations. Among all the wide band gap devices, AlGaN/GaN HEMT becomes the favorable choice due to its large internal gain resulting from the highly conductive 2DEG channel leading to high mobilities and carrier densities. Among various devices in the semiconductor domain, the GaN HEMTs exhibits the best detectivities and hence has great potential to be used as a rugged UV detector [9-11]. However, all these works focus on diode structures achieving high detectivities. Only a very few works in literature focuses on transistor-based detector, the major reason being the increased cost and product complexities [8]. The advantage of using transistor-based detector is that the photocurrent gets amplified by the transistor gain factor yielding higher responsivities and detectivities. Presented here is a systematic approach towards development of a UV detector where simulation models are developed and used so that the fabrication costs, time, costs and resource overheads can be minimized. Such methods of modeling prior to fabrication have been employed in transistor-based chemical and bio sensor design but has not been used till date in photo detector simulations [6, 12-15]. This work presents the use of optical module in Silvaco ATLAS TCAD to simulate the device performance as a UV detector followed by fabrication and characterization of the detector along with its fabrication and characterization. Si has been used as the substrate here to reduce the cost of the sensors favoring its commercialization in future.

The detector presented here exhibits better sensitivity as well as detectivity due to high end HEMT technology used here

which is like the modern-day RF-HEMTs that are currently in research. This high response in the device can be attributed to the amplification of channel currents due to the photovoltage generated which is a function of the illumination wavelength. The devices presented here have been developed with focus on application in harsh environments such as in space and military application, hence they are equipped with a source field plate which enhances the device reliability while slightly helping in increase of detection through the slight enhancement in drain current and transconductance (g_m). The field plate length however is limited to the gate, extending slightly over it as the area from gate to drain can be fully opened for UV illuminations. This Field plate enhances the device reliability and makes it robust for use in harsh environments. The recombination's that occur in the channel with UV illumination are demonstrated which explains the transportation mechanism of the photogenerated carriers. Further, the impact of device dimensions on responsivity has been evaluated through fabrication and testing of devices with variable W/L ratios. All these devices are fabricated with a source field plate Gate to drain distance (L_{GD}) > 2 x Source to gate distance (L_{SG}) to ensure that this high responsive UV detectors comes with high breakdown voltages. These devices can further be tailored through tuning of AlGaN band gaps by varying the Al mole fraction or through a change in the barrier materials to develop selective wavelength detections for present and futuristic space explorations.

II. SIMULATION: METHODS AND MODELS

AlN spacer used between AlGaN/GaN layers have shown to improve the performance of the HEMTs, in DC, RF and sensing domains [6, 14, 16, 17]. This technology is made use here to get detectors with enhanced. The epitaxial stack used and the conduction band bending at the interface leading to the 2DEG channel formation is depicted in Fig. (1). The device has been simulated using NEWTON method in SILVACO ATLAS TCAD. Inbuilt concentration dependent mobility models along with GaN specific GANSAT model has been used for accurate modeling of device mobility. Further, recombination models such as AUGER, SRH and CONSRH models has been used to model the recombination along with ALBRCT model for impact ionization. The ohmic metal stack has been simulated as a conductor with work function of 5.15 eV and the Schottky gate with an equivalent work function of 4 eV. The device width used is 125 μm and the outputs are then normalized to 100 μm device width to ease the calibration, and comparisons with works in literature. Device dimensions used are summarized in Table. I. UV detection has been simulated by incorporating optical modules in SILVACO simulations. The conduction band bending deeper below the Fermi level thereby increasing the conduction band offset and hence the 2DEG density is presented in Fig. 2. (a), the corresponding increase in 2DEG is shown in Fig. 2. (b). It has been observed from the simulation results that the 2DEG is not only increased but also shifted linearly with UV illumination.
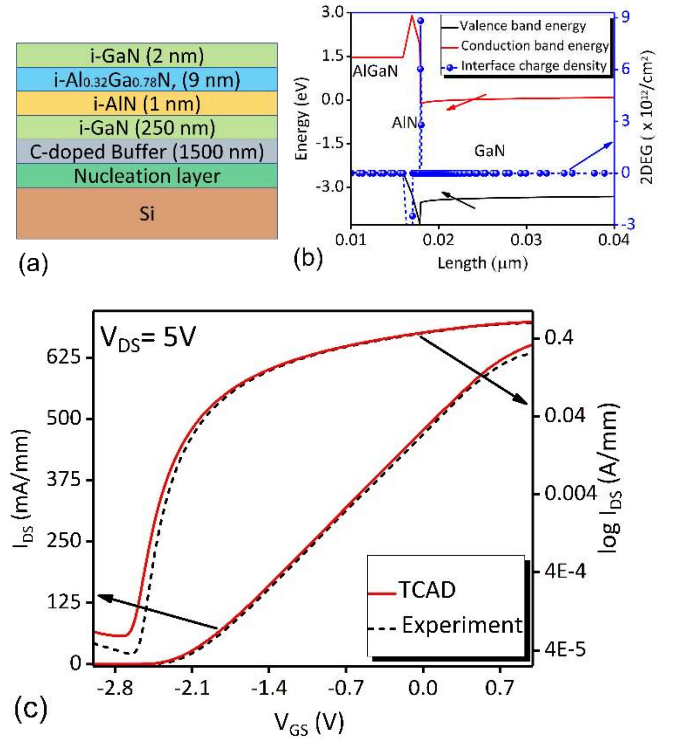

Fig. 1. (a). Cross sectional schematic of AlGaN/GaN HEMT stack, (b). Energy band diagrams and interface charge density at the hetero interface, (c). Calibration and validation of TCAD models, comparison with experiment.

TABLE I
DEVICE DIMENSIONS AND SIMULATION PARAMETERS

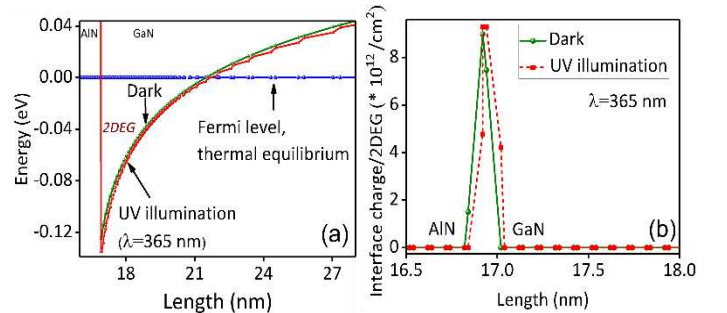| Symbol	Parameter	Value
L_{SG}	Source to Gate distance	1.5 μm
L_G	Gate length	1 μm
L_{GD}	Gate to Drain distance	17.5 μm
Vsat (AlGaN)	AlGaN saturation velocity	1.165×10^7 cm/s
Vsat (AlN)	AlN saturation velocity	2.167×10^7 cm/s
Vsat (GaN)	GaN saturation velocity	1.906×10^7 cm/s
W	Device width	125 μm

Fig. 2. (a). Deepening of 2DEG with UV illumination, (b). resultant interface charge density.

III. FABRICATION AND CHARACTERIZATION

The HEMT epi stacks were grown on Si substrate using Metal Organic Chemical Vapor Deposition (MOCVD). The thin $Al_{0.32}Ga_{0.78}N$ barrier layer was grown on 250 nm unintentionally doped GaN channel and 1500 nm C-doped GaN buffer with a thin 1 nm AlN spacer. The epi layer stack exhibited an average mobility of 2786 cm^2/V. s with 2DEG density of 9.08 x 10^{12} /cm^2 in Vander Pauw Measurements (VDP). Standard fabrication flow was followed beginning with ohmic metallization, where 20 nm/120 nm/40 nm/50 nm of Ti/Al/Ni/Au was deposited. The mesa isolation was achieved using Cl$_2$ based ICP-RIE. PECVD based nitride deposition has been used for device passivation. The gate Schottky contacts of 20 nm/200 nm of Ni/Au were deposited using e-beam evaporation followed by field plate metallization. Similar fabrication processes and tools are used as detailed in [18].

For UV illumination, LED lamp from FACOM has been used they come with fixed wavelengths in different ranges and constant power of 1W. The UV of HEMT is expressed as:

$$Responsivity = \frac{I_{ph}}{Optical\ power} \qquad (1)$$

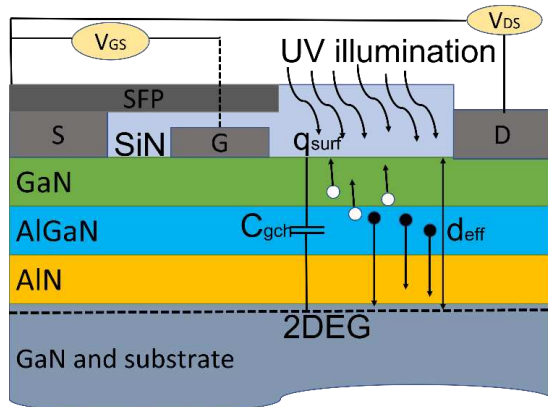the total area to the active device area. i.e. if the total beam area is Πr^2 and the total device area is total device length multiplied by its width, then total power falling on the device is estimated as:

$$Optical\ power\ (W) = 1 \times \frac{\pi r^2}{length \times width} \qquad (2)$$

Optical power incident on the active area of the device has been obtained by comparison of total active area of incidence to the active device area [8]. The optical power falling on the active device area of 125 $\mu m * 212\ \mu m$ is ~2.5 x 10^{-10} W. The photocurrents of the UV detector at UV wavelengths of 365 nm and 395 nm are depicted in Fig. 6 (a) and (b). These currents are obtained as the difference in illumination currents from the dark currents presented in Fig. 6 (c) and (d). The detectivity falls as the wavelength increases making the detectors blind to visible lights. This ensures selective detection of UV radiations when GaN based detectors are used. Schematic representation for the experimental set up and power estimation is shown in Fig. 5.

Fig. 3. Cross section of the fabricated device demonstrating the UV detection mechanism.
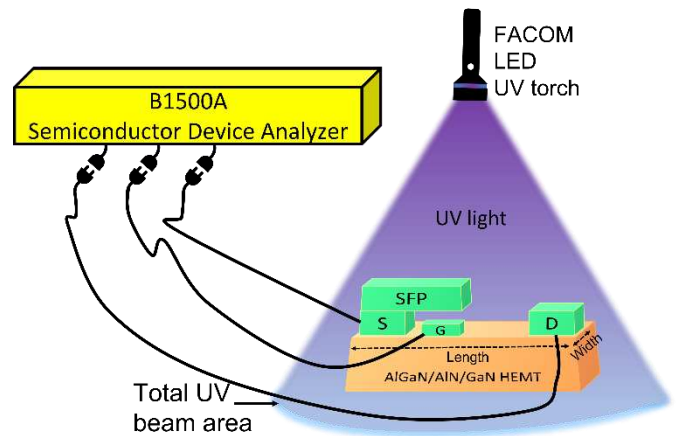
Fig. 5. Schematic representation of UV detection showing the active device area and the total UV area used in power estimation.

Where I_{ph} is the photo current, which is the variation in output current in response to UV illumination. The total optical power falling on the device has been calculated by comparing

IV. RESULTS AND DISCUSSION

The total optical power incident on the detector is $\sim 25\ nW$.

Fig. 4. Top view of the fabricated HEMT with source field plate extending over the gate, the FP to gate Si$_3$N$_4$ separation is 100 nm and the the FP to gate Si$_3$N$_4$ separation is 300 nm.

The illumination current in the device output is expressed as:

$$I_{ill} = I_D + \Delta I_D = I_D + I_{ph} \qquad (3)$$

$$I_{ill} = q \times (n_s \pm \Delta n_s) \times W \times V(x) \qquad (4)$$
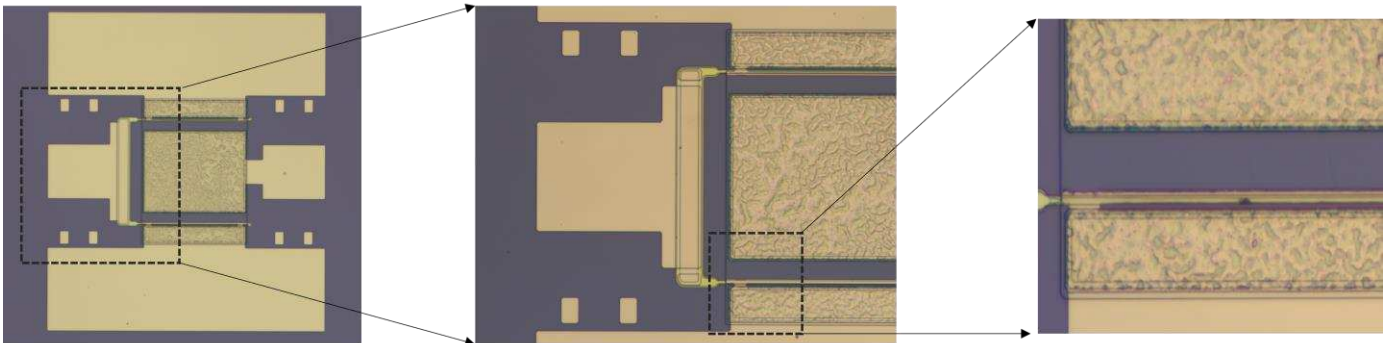
Where q is the electron charge, n_s is the change in 2DEG density with UV illumination induced by the photo voltage generated by the surface charges forming a virtual gate. This surface charges are counterbalanced by the change in 2DEG density Δn_s thus leading to an effective variation in device current, ΔI_D also called photo current I_{ph}.

$$V_{UV} = \frac{q_{surf}}{C_{gch}} \qquad (5)$$

Where q_{surf} is the surface charge, the effective variation in 2DEG can be modeled as capacitive coupling of this surface charge to the device channel as expressed in eqn. (5). Here C_{gch} is the effective capacitance density per unit area between the surface and the 2DEG location below the AlN layer. The separation of the surface charge to the 2DEG is contributed by the combined thicknesses of GaN cap layer (t_{cap}) AlGaN barrier (t_{AlGaN}), thickness of the spacer layer (t_{AlN}), and the offset of 2DEG from the interface (Δd_{2DEG}) as depicted in Fig. (9).

$$d_{eff} = t_{cap} + t_{AlGaN} + t_{AlN} + \Delta d_{2DEG} \qquad (6)$$

$$I_{ph} = V_{UV} \times g_m \qquad (7)$$

g_m is the device transconductance, i.e. expressed as $\partial I_D / \partial V_{GS}$. V_{UV} is the photovoltage generated on the device surface which acts on the device as a virtual positive gate bias applied. This can be expressed in terms of photocurrent density and lifetime of holes on the device surface.

$$V_{UV} = \frac{J_{UV} \times \tau_{lh}}{C_{gch}} \qquad (8)$$

Where J_{UV} is the surface current density and τ_{lh} is the life time of holes which can be analyzed through evaluation of recombination rates in simulation.
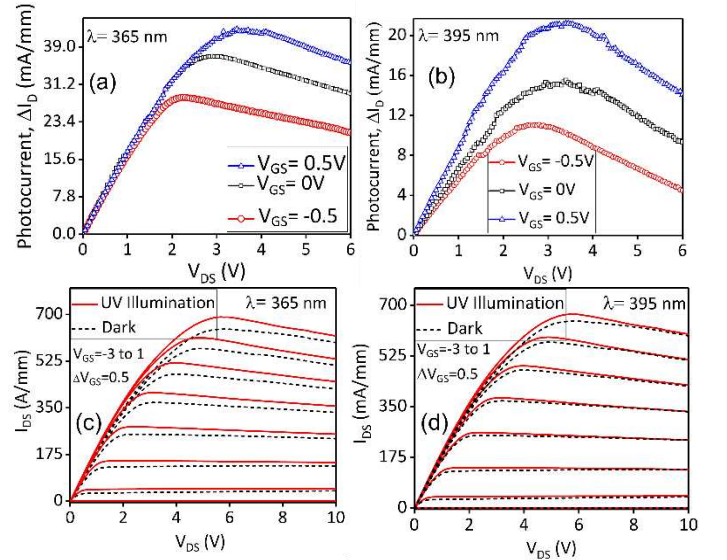

Fig. 5. (a). Photocurrent for 365 nm UV illumination, (b). Photocurrent for 395 nm UV illumination, (c). Illumination and dark currents, 365 nm, (d). Illumination and dark currents, 395 nm.

The recombination rates near the channel area in the gate to drain region under dark and illumination conditions have been simulated and plotted using a horizontal cutline is presented in Fig. 7. The effective hole generation rate can be assumed similar to the recombination rate. The illumination current I_{ill} which acts as the reference current is expressed in terms of Electric Field E(x) in eqn. (8) [16]. Where ϵ_{AlGaN} is the relative permittivity of AlGaN barrier, V_{GS} is the bias applied on the Schottky gate, $\emptyset_s$ is the Schottky barrier height, E_F is the Fermi energy, ΔE_{cAlGaN} is the conduction band bending induced through formation of virtual gate at the surface, σ_{AlN} is the charge density in AlN spacer due to spontaneous and piezoelectric polarization, $V_{ch}(x)$ is the channel potential at distance x in the device channel, v_s and μ are the saturation velocity and low field mobility in the channel respectively.

$$I_{ill} = q \frac{\epsilon_{AlGaN}}{d_{eff}} \left(V_{GS} - \left(\emptyset_s + \frac{E_F - \left(\Delta E_{cAlGaN}\ (m) + \frac{q^2}{\epsilon_{AlGaN}\ (m)} \sigma_{AlN}{}^2 t_{AlN} \right)}{q} + V_{ch}(x) \right) \right) \times W \times \frac{v_s E(x)}{\sqrt{E^2(x) + \left(\frac{v_s}{\mu} \right)^2}} \pm V_{UV} \times g_m \qquad (9)$$

Substituting (8) in (9), the illumination current becomes:

$$I_{ill} = q \frac{\epsilon_{AlGaN}}{d_{eff}} \left(V_{GS} - \left(\emptyset_s + \frac{E_F - \left(\Delta E_{cAlGaN}\ (m) + \frac{q^2}{\epsilon_{AlGaN}\ (m)} \sigma_{AlN}{}^2 t_{AlN} \right)}{q} + V_{ch}(x) \right) \right) \times W \times \frac{v_s E(x)}{\sqrt{E^2(x) + \left(\frac{v_s}{\mu} \right)^2}} \pm \frac{J_{UV} \times \tau_{lh}}{C_{gch}} \times g_m \qquad (10)$$
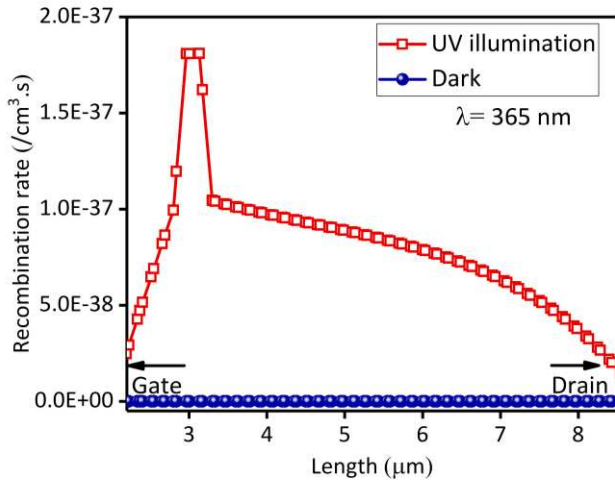
Fig. 7. Recombination rate in the near channel region below the sensing area (area between the gate and drain).

Bandgap of top AlGaN with Al mole fraction of 0.32 is ~3.985 eV, hence maximum responsivity is observed in UV-A region and the responsivity falls to zero as the wavelength approaches the visible light wavelength. Further, the transparent nature of the layers also allows for some radiations to pass through and excite the carriers in the narrow band gap GaN layer too. This makes the device work as visible blind detectors with peak responsivity of 1.62×10^7 A/W at V_{GS}=0.5 V, and V_{DS}=3.5 V.
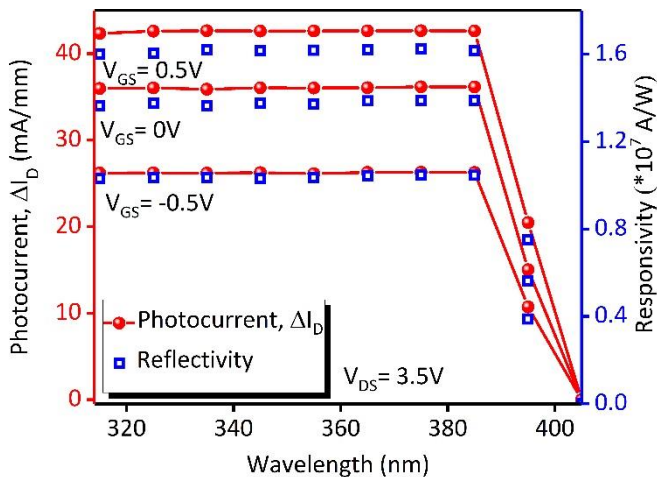

Fig. 8. Photocurrents and responsivities of the detector at different gate bias.

V. IMPACT OF W/L ON DETECTOR PERFORMANCE

The area available for incidence of UV radiations has a huge impact on the detector performance. It has been observed that the responsivity increases as the area is increased. To analyze the impact of W/L on performance, the gate length, as well as spacings from source to drain are maintained the same while changing the device widths.
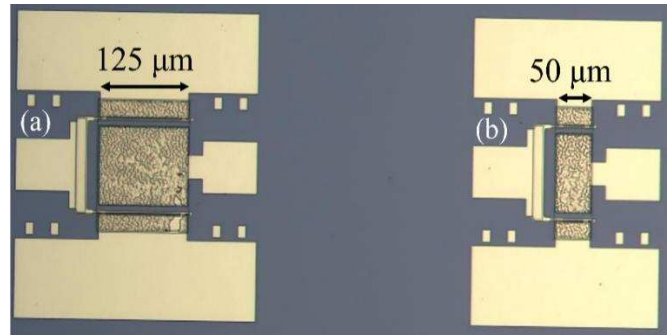

Fig. 9. Device with variant active area widths of 125 μm and 50 μm.

Fig. 9 presents two detectors with different active area widths. The increase in responsivities with increase in area is shown in Fig. 10. The characteristics flattens as the W/L ratio increased over 150. The device exhibits enhanced performance over the GaN based counterparts as well as the other material systems. A short summary of the comparison with other photodetectors from the recent literature is presented in Table. II and Table. III. The device exhibits better performance than other HEMT based systems due to the modifications in device design brought in to enhance the gm and internal gain. The internal gain in the HFET based systems makes all of them provide better response over the conventional heterojunction-based detectors presented in Table. III.
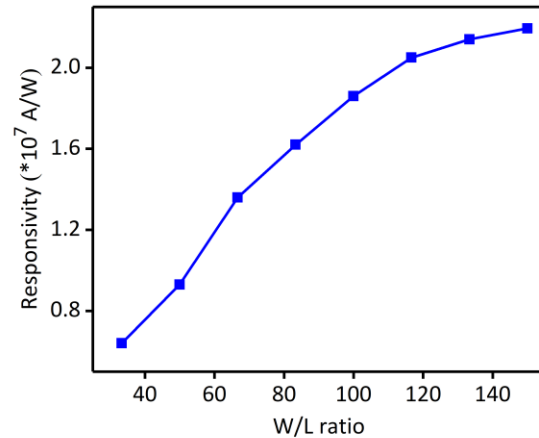

Fig. 10. Increase in device responsivity with increase in W/L ratio.

VI. CONCLUSION

Field plated AlGaN/AlN/GaN HEMTs have been used as visible blind UV detectors and performance analysis has been done for different UV wavelengths. Experimental analysis has been backed with simulation-based investigations using TCAD based models and an analytical model development. The fabricated devices outperforms the existing detectors with responsivities of 1.6×10^7 A/W at UV wavelengths of 365 nm. The impact of W/L on responsivity has been analyzed by varying the device widths and it has been observed that the responsivity increases as the width increases and it saturates. The responsivity initially increases by 98 % as the device width is increased from 50 μm to 100 μm, further increase in width do not impact the responsivity much as only 18 % enhancement is observed as the device width is increased from

TABLE II
COMPARISON WITH OTHER GAN HFET-BASED DETECTORS

Device	g_m (mS/mm)	UV Wavelength (nm)	Spectral Responsivity (A/W)	V_{GS} (V)	Optical Power (W)
AlGaN/AlN/GaN HEMT (**This work**)	228	365	1.6×10^7	0.5	2.5×10^{-10}
InAlN/AlN/GaN MOS-HFET [19]	180.4	350	360	5	36×10^{-6}
AlGaN/GaN HEMT [8]	-	365	4.3×10^7	0	50×10^{-12}
InGaN/GaN HFET [20]	-	365	470	3	160×10^{-6}

HFET: Heterojunction Field Effect Transistor, FP: Field Plate

TABLE III
COMPARISON WITH GAN AND OTHER MATERIAL HETEROSTRUCTURES BASED DETECTORS FROM 2021

Device	Photocurrent range	UV Wavelength (nm)	Spectral Responsivity (A/W)	Optical Power/Intensity (W)
Source FP AlGaN/AlN/GaN HEMT (**This work**)	milliamps	365	1.6×10^7	2.5×10^{-10}
PdTe$_2$/GaN hetj [21]	microamps	265	168.5×10^{-3}	1.53×10^{-3} /cm^2
ZrGaO/n-GaN hetj [22]	microamps	362	33.3	270×10^{-6} /cm^2
MoS$_2$/Al$_2$O$_3$/CuO hetj [23]	microamps	302	1.33	12.9×10^{-6} /cm^2
Ga$_2$O$_3$/BiFeO$_3$ hetj [24]	nanoamps	254	$\sim 100 \times 10^{-3}$	200×10^{-6} /cm^2
p-NiO/n-GaZnO hetj [25]	microamps	300	0.18	20×10^{-6}
Ti/Ga$_2$O$_3$/Ti MSM [26]	microamps	254	139.56	2000×10^{-6} /cm^2

Hetj: heterojunction, MSM: Metal-Semiconductor-Metal

100 µm to 150 µm. Comparison with existing diode and transistor-based detectors shows that the proposed devices exhibits performance enhancement ratios of 10's to 1000's of magnitude respectively. The model presented here can be used to perform systematic analysis prior to the fabrication of UV detectors and the proposed device with its large responsivity proves its promise to be used as a visible blind UV detector. The performance of these devices can be further improved by optimizing the channel growth conditions.

REFERENCES

[1]. Y. Ando, R. Makisako, H. Takahashi, A. Wakejima, and J. Suda, Dependence of Electrical Characteristics on Epitaxial Layer Structure of AlGaN/GaN HEMTs Fabricated on Freestanding GaN Substrates. *IEEE Trans. on Electron Dev.*, pp. 1-8, Nov. 2021, doi: 10.1109/TED.2021.3126270

[2]. H. Wang, W. Mao, C. Yang, J. Chen, S. Zhao, M. Du, X. Wang, X. Zheng, C. Wang, C. Zhang, and J. Zhang, Lateral AlGaN/GaN Schottky Barrier Diode with Arrayed p-GaN Islands Termination. *IEEE Trans. on Electron Dev.*, vol. 68, no. 12, pp. 6046-6051, Oct. 2021, doi: 10.1109/TED.2021.3118326.

[3]. A. M. Eblabla, X. Li, D. J. Wallis, I. Guiney, and K. Elgaid, GaN on low-resistivity silicon THz high-Q passive device technology. *IEEE Transactions on Terahertz Science and Technology*, 7(1), pp.93-97, 2016, doi: 10.1109/TTHZ.2016.2618751.

[4]. H. Chandrasekar, M. J. Uren, M. A. Casbon, H. Hirshy, A. Eblabla, K. Elgaid, J. W. Pomeroy, P. J. Tasker, and M. Kuball, Quantifying temperature-dependent substrate loss in GaN-on-Si RF technology. *IEEE Transactions on Electron Devices*, 66(4), pp.1681-1687, 2019, doi: 10.1109/TED.2019.2896156.

[5]. C. L.Tsai, T. W. Wang, Y. C. Li, A. Das, C. W. Chen, Y. J. Chen, and S. C. Ko, Underwater optical wireless communications with InGaN LEDs grown with an asymmetric multiple quantum well for light emission or detection. *IEEE Photonics Journal*, 2021, doi: 10.1109/JPHOT.2021.3130133.

[6]. A. Varghese, A. Eblabla, and K. Elgaid, Modeling and Simulation of Ultrahigh Sensitive AlGaN/AlN/GaN HEMT based Hydrogen gas

[7]. detector with low detection limit. *IEEE Sensors Journal*, vol. 21, no. 13, pp. 15361-15368, Jul. 2021, doi: 10.1109/JSEN.2021.3072476.

[7]. H. So, J. Lim, and D. G. Senesky, Continuous V-grooved AlGaN/GaN surfaces for high-temperature ultraviolet photodetectors. *IEEE Sensors Journal*, 16(10), pp.3633-3639, 2016, doi: 10.1109/JSEN.2016.2531181.

[8]. Z. H. Zaidi, and P. A. Houston, Highly sensitive UV detection mechanism in AlGaN/GaN HEMTs. *IEEE Transactions on electron devices*, 60(9), pp.2776-2781, 2013, doi: 10.1109/TED.2013.2273618.

[9]. M. A. Khan, M. S. Shur, Q. Chen, J. N. Kuznia, and C. J. Sun, Gated photodetector based on GaN/AlGaN heterostructure field effect transistor, Electron. Lett., vol. 31, no. 5, pp. 398–400, Mar. 1995, doi: 10.1049/el:19950247.

[10]. B. Poti, M. T. Todaro, M. C. Frassanito, A. Pomarico, A. Passaseo, M. Lomascolo, R. Cingolani, and M. De Vittorio, "High responsivity GaN-based UV detectors," Electron. Lett., vol. 39, no. 24, pp. 1747–1749, Nov. 2003.

[11]. M. Martens, J. Schlegel, P. Vogt, F. Brunner, R. Lossy, J. Würfl, M. Weyers, and M. Kneissl, "High gain ultraviolet photodetectors based on AlGaN/GaN heterostructures for optical switching," Appl. Phys. Lett., vol. 98, no. 21, pp. 211114-1–211114-3, May 2011, doi: 10.1063/1.3595303.

[12]. M. Moser, M. Pradhan, M. Alomari, and J. N. Burghartz, Model and Simulation of GaN-Based Pressure Sensors for High Temperature Applications—Part I: Physics Based Compact Modeling. *IEEE Sensors Journal*, 21(18), pp.20165-20175, 2021, doi: 10.1109/JSEN.2021.3096206.

[13]. P. Pal, Y. Pratap, M. Gupta, and S. Kabra, Analytical Modeling and Simulation of AlGaN/GaN MOS-HEMT for High Sensitive pH Sensor. *IEEE Sensors Journal*, 2021, doi: 10.1109/JSEN.2021.3069243.

[14]. A. Varghese, C. Periasamy, and L. Bhargava, Analytical modeling and simulation-based investigation of AlGaN/AlN/GaN bio-HEMT sensor for C-erbB-2 detection, *IEEE Sensors J.*, vol. 18, no. 23, pp. 9595–9603, Dec. 2018, doi: 10.1109/JSEN.2018.2871718.

[15]. A. M. Bhat, N. Shafi, C. Sahu, and C. Periasamy, AlGaN/GaN HEMT pH Sensor Simulation Model and Its Maximum Transconductance Considerations for Improved Sensitivity. *IEEE Sensors Journal*, 21(18), pp.19753-19761, 2021, doi: 10.1109/JSEN.2021.3100475.

[16]. A. Varghese, C. Periasamy, L. Bhargava, and K. Vijayakumar, Impact of AlN interlayer's in epitaxial and passivation scheme on the DC and microwave performance of doping-less GaN HEMT, *J. Nanoelectron.*

Optoelectron., vol. 13, no. 7, pp. 971–979, Jul. 2018, doi: 10.1166/jno.2018.2308.

[17]. C. Wang, X. Wang, G. Hu, J. Wang, J. Li, and Z. Wang, Influence of AlN interfacial layer on electrical properties of high-Al-content Al0. 45Ga0. 55N/GaN HEMT structure. *Applied Surface Science*, vol. 253, no. 2, pp.762-765, Nov. 2006, doi: 10.1016/j.apsusc.2006.01.017.

[18]. B. Benakaprasad, A. M. Eblabla, X. Li, K. G. Crawford, and K. Elgaid, K., Optimization of ohmic contact for AlGaN/GaN HEMT on low-resistivity silicon. *IEEE Transactions on Electron Devices*, 67(3), pp.863-868, Mar, 2020, doi: 10.1109/TED.2020.2968186.

[19]. C. -S. Lee, X. -C. Yao, Y. -P. Huang and W. -C. Hsu, Improved Ultraviolet Detection and Device Performance of Al_2O_3-Dielectric $In_{0.17}Al_{0.83}N$/AlN/GaN MOS-HFETs, *IEEE Journal of the Electron Devices Society*, vol. 7, pp. 430-434, 2019, doi: 10.1109/JEDS.2019.2906354.

[20]. Z. Lv, Z. Liao, and H. Jiang, InGaN/GaN Visible-Light Heterojunction Phototransistor Featuring High Responsivity, High Speed, and Bias-Controlled Wavelength-Selectivity. *IEEE Electron Device Letters*, 42(9), pp.1362-1365, 2021, doi: 10.1109/LED.2021.3097048.

[21]. Y. Liang, M. Ma, X. Zhong, C. Xie, X. Tong, K. Xing, and C. Wu, Multilayered PdTe2/GaN Heterostructures for Visible-Blind Deep-Ultraviolet Photodetection. *IEEE Electron Device Letters*, 2021, doi: 10.1109/LED.2021.3087704.

[22]. J. Guo, M. Ma, Y. Li, D. Zhang, Y. Liu, and W. Zheng, Bandgap Engineering of ZrGaO Films for Deep-Ultraviolet Detection. *IEEE Electron Device Letters*, 42(6), pp.895-898, 2021, doi: 10.1109/LED.2021.3070899.

[23]. R. Singh, and S. Tripathi, Low Intensity UV Light Detection by Al 2 O 3 Separated MoS 2/CuO Junction. *IEEE Photonics Technology Letters*, 33(24), pp.1427-1430, 2021, doi: 10.1109/LPT.2021.3122803.

[24]. G. L. Ma, A. Gao, Z. Liu, W. M. Sun, S. Li, Z. Y. Yan, W. Y. Jiang, B. Y., Sun, X. H. Qi, P. G. Li, and W. H. Tang, Solution Spin-Coated BiFeO 3 Onto Ga 2 O 3 Towards Self-Powered Deep UV Photo Detector of Ga 2 O 3/BiFeO 3 Heterojunction. *IEEE Sensors Journal*, 21(21), pp.23987-23994, 2021, doi: 10.1109/JSEN.2021.3115719.

[25]. H. Y. Liu, and Z. Y. Huang, Investigation of p-NiO/N-Ga$_{0.3}$Zn$_{0.7}$O Heterojunction Photodiodes for Ultraviolet-B Detection. *IEEE Sensors Journal*, 21(19), pp.21486-21493, 2021, doi: 10.1109/JSEN.2021.3104826.

[26]. Y. S. Zhi, Z. Liu, S. H. Zhang, S. Li, Z. Y. Yan, P. G. Li, and W. H. Tang, 16x 4 Linear Solar-Blind UV Photoconductive Detector Array Based on β-Ga$_2$O$_3$ Film. *IEEE Transactions on Electron Devices,* 2021, doi: 10.1109/TED.2021.3081522.

Abdalla Eblabla Abdalla Eblabla received the B.S. degree in communication engineering from Misurata University, Misurata, Libya, in 2008, the M.S. degree in electronics and electrical engineering from the University of Glasgow, Glasgow, U.K., in 2012, and the PhD degree in electronics and electrical engineering from the University of Glasgow, Glasgow, U.K., in 2018.

He is currently a Lecturer of the Centre for High-Frequency Engineering (CHFE) with Cardiff University, Cardiff, U.K. His research interests include design, fabrication, and characterization of microwave and millimeter wave components and circuit design using nitride based III-V semiconductors technology.

Zehao Wu received the B.Sc. degree in Computer Science and Technology from East China University of Science and Technology, China, in 2013, and the M.Sc. degree in Computer Systems Engineering from the University of Glasgow, U.K., in 2017. He is currently working toward the Ph.D. degree in electronic and electrical engineering at Cardiff University. His research interests include MMIC circuit design and modeling and fabrication of semiconductor devices.

Seyed Urman Ghozati received received the B.Eng. degree in Electronics, and his first M.Sc. degree in Electrical Power engineering from Northumbria University, Newcastle, in 2018 and his second M.Sc. degree in compound semiconductor electronics from Cardiff University, Cardiff, in 2020, where he is currently pursuing a PhD degree with Centre for High Frequency Engineering (CHFE) at Cardiff University. His current works include design and simulation, characterization, modelling of RF GaN semiconductor devices.

Arathy Varghese received her B.Tech degree in Electronics and Communication Engineering from Kerala University, India, in 2013, M.Tech degree in VLSI and Embedded System from the Mahatma Gandhi University, Kerala, India, in 2015, and PhD degree in Electronics and Communication Engineering from Malaviya National Institute of Technology Jaipur, Rajasthan, India, in 2020. She is currently working as Research Associate with the School of Engineering, Cardiff University, Wales, U.K. Her research interests include simulation and modeling of semiconductor devices, and development of micro and nano electronic devices for high power, high frequency, and sensing applications.
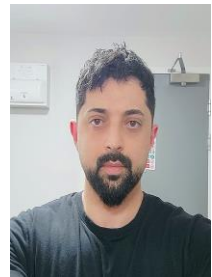
Khaled Elgaid received his B.Sc. from University of Evansville, USA, M.Sc. from Marshall University, USA, M.Sc. from The University of Cincinnati, USA, and Ph.D. from The University of Glasgow, UK. He is currently holding a professor post at Cardiff University, UK, leading a High-Speed Integrated Electronics Technology research team in compound semiconductor with a focus on GaN and emphasises in high data rate telecommunications, sensors and radar applications. He has more than 25 years' experience in micro and nano technology for developing integrated electronic active and passive devices and MMIC technology with frequencies operating up to THz.